



University of
Massachusetts
Amherst

Handheld Device for Burn Depth Analysis Through Skin Hydration: A Proof of Concept

Item Type	Thesis (Open Access)
Authors	Newhall, Erin
DOI	10.7275/ard6-z845
Rights	Attribution-NonCommercial 4.0 International
Download date	2026-05-20 17:07:29
Item License	http://creativecommons.org/licenses/by-nc/4.0/
Link to Item	https://hdl.handle.net/20.500.14394/56671

Handheld Device for Burn Depth Analysis Through Skin Hydration: A Proof of Concept

A Thesis Presented
by
ERIN M NEWHALL

Submitted to the Graduate School of the University of Massachusetts Amherst in partial
fulfillment of the requirements for the degree of

MASTER OF SCIENCE

May 2025

Biomedical Engineering

Handheld Device for Burn Depth Analysis Through Skin Hydration: A Proof of Concept

A Thesis Presented

by

ERIN M. NEWHALL

Approved as to style and content by:

Martin Hunter, Chair

Joyita Dutta, Graduate Program Director
Department of Biomedical Engineering

ABSTRACT

HANDHELD DEVICE FOR BURN DEPTH ANALYSIS THROUGH SKIN HYDRATION

MAY 2025

ERIN NEWHALL, B.S., UNIVERSITY OF MASSACHUSETTS AMHERST

M.A., UNIVERSITY OF MASSACHUSETTS AMHERST

Directed by: Professor Martin Hunter

About 500,000 Americans seek treatment for burns annually, but burn depth, used to create treatment plans and determine whether surgery is needed for treatment, is only correctly found about 50-80% of the time in the US. In the UK and other countries, clinicians have used laser doppler imaging (LDI) with clinical evaluation to increase diagnostic accuracy, however US based physicians tend to just use clinical evaluation, citing cost and difficulty of use as reasons for not using this technology. The purpose of this thesis is to present an innovative, cheap, and easy to use device that can be used to evaluate burn depth in a non-contact modality.

When researching the pathophysiology of burn injuries, I found Jackson's thermal wound theory, postulating that besides the degradation of proteins in the immediate environment, poor fluid flow is the next biggest challenge, without fixing more tissue will die. LDI uses this idea to look for fluid movement, while I planned to use this by finding water. The macro scale seemed to support this as well, burn victims with a significant amount of skin area burned lose so much fluid that they require IV fluid resuscitation for recovery. Based on this detection method, I created a device with a pair of LEDs that emit light at 910 and 970 nm, where 970 nm is a water absorption peak. To ensure that the device meets standards, a mathematical model was created and tested.

TABLE OF CONTENTS

	Page
ABSTRACT.....	iii
LIST OF TABLES.....	v
LIST OF FIGURES.....	vi
CHAPTER	
1. THE CASE FOR BETTER BURN DEPTH DETERMINATION.....	1
1.1 Burns.....	1
1.2 Current Methods.....	2
1.3 Methods in Development.....	2
2. BURN DEPTH AND SKIN HYDRATION.....	5
2.1 Jackson Thermal Wound Theory.....	5
2.2 Other Examples of Water Loss from Burns.....	5
2.3 Noninvasive Methods of Measuring Water Content.....	6
3. PROPOSED DEVICE.....	9
3.1 Materials.....	9
3.2 Circuit.....	10
4. SAFETY OF PROPOSED METHOD.....	11
4.1 Introduction.....	11
4.2 Irradiance Equations	11
4.2.1 Defining the Area	12
4.3 Radiance Equations.....	14
5. PLANNED TESTING.....	17
5.1 Hydration testing.....	17
5.2 Skin testing.....	17
5.3 Conclusion.....	18
BIBLIOGRAPHY.....	19
APPENDICES	
A. Code used in each experiment.....	20
B. List of equations used.....	21
B.1 Equations from IEC-62471.....	21
B.2 Optical Equations.....	21

LIST OF TABLES

Table	Page
1. Features of discussed methods to assess burn depth [9]	4

LIST OF FIGURES

Figures	Page
1. Representation of burn depth on skin diagram [1].....	1
2. The zones of Jackson's thermal wound theory [2].....	5
3. Some symptoms of burn shock [2].....	6
4. Methods of measuring skin hydration [3].....	7
5. From left to right, absorption coefficients of liquid water [4] and the absorbance of chromophores in skin within the proposed range, adapted from [5].....	8
6. Responsivity curve from photodiodes used, provided in product information.....	9
7. Original device circuit	10
8. Modified photodiode circuit	10
9. (1), (2), and (3) plotted.....	11
10. Pictorial representation of important variables used in (10) [6].....	13
11. Irradiance per distance for an LED with a power of 16 mW and a dispersion angle of 14° , where distance is defined as that between the virtual image and the surface.....	14
12. From left to right, the irradiance from the maximum optical power from each LED at various distances from tissue, the maximum amount of time considered to be safe to look at the LED per the radiance equations using values provided by the LED manufacturer at various distances from the eye.....	16

CHAPTER 1

THE CASE FOR BETTER BURN DEPTH DETERMINATION

1.1 Burns

Burns cause over 400,000 emergency room visits in America alone [7]. They are generally classified into several different causes: flame, contact with hot objects (scalds, contact burns), electricity, chemicals, and radiation [1]. While they all have similar signs and symptoms, some pathologies present differently depending on burn cause. For the purposes of this thesis, I will be looking exclusively at flame burns, contact burns, and scalds. Burns are commonly also classified by their depth, or the layers of skin damaged by the injury. These had previously been known as burn degree (1st degree, 2nd degree, 3rd degree), but are now also known by to what extent they penetrate the dermis. Superficial (1st degree) burns do not damage the dermis, and a common example is mild sunburns, where the sun's radiation only damages the upper skin layer (epidermis). Partial thickness (2nd degree) and full thickness (3rd degree) burns either partially or completely damage the integrity of the dermal barrier, as shown below.

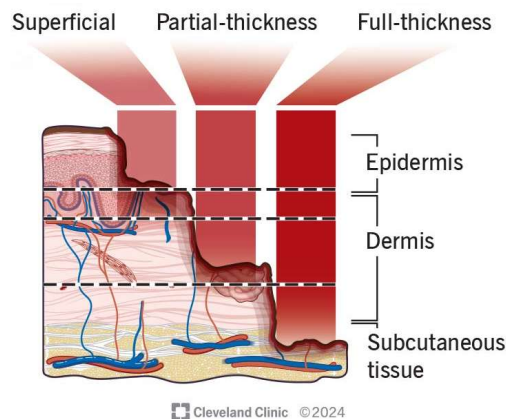


Figure 1: Representation of burn depth on skin diagram [1]. As discussed above, superficial burns only damage the epidermis, but do not damage lower layers, blood vessels, or nerves. Meanwhile, partial thickness burns destroy part of the dermis, damaging blood vessels and potentially nerve fibers depending on how deep the burn is in the dermis. Once the burn damages the subcutaneous layer (full thickness), it has damaged blood vessels, nerves, and the stem cells at the bottom layer of the dermis that regenerates dermal and epidermal cells. At this point, for best chances of healing and better quality of life, a skin graft is needed.

There are some differences between partial thickness and full thickness signs and symptoms, however these differences become more difficult to see as a partial thickness burn approaches a full thickness burn, as nerve damage can occur with deep partial thickness burns. Evidence of nerve damage can lead providers to wrongly assume the patient has a full thickness burn, leading to more expensive treatment for the patient.

1.2 Current Methods

In America, most treatment centers use signs and symptoms to determine burn depth. As mentioned in the last section, partial and full thickness burns are difficult to differentiate between, especially in the case of deep partial thickness burns. In a 2014 study looking at burn treatment centers, researchers found that some of the most commonly cited reasons for centers not using well researched equipment to aid in determining burn depth was cost of equipment and difficulty of use [8]. In the same study, they also found that trained and experienced burn clinicians had an accuracy of correctly determining burn depth ranging from 50 to 80%, perhaps partly owing to the difficulty of differentiating between partial and full thickness burns by signs and symptoms alone.

1.3 Methods in Development

Many different burn depth analysis methods have been proposed and tested to various degrees of success. Outside of America, laser doppler imaging (LDI) has become increasingly popular in burn clinics [9]. LDI looks at blood perfusion of burn tissue, and has been found to be more accurate than clinical assessment when used between 48 and 120 hours post injury, but lacks standards for measurement and takes 1 to 2 minutes to complete a scan of an area of up to 2500 cm²[10]. There are some developments on trying to speed this process up, as during the scan, the patient should not move as this can give conflicting data.

As of 2024, no other technologies have been integrated into burn clinics, however many are in development. Similar to LDI in parameters measured, laser speckle imaging (LSI) compares backscatter of burn tissue to static tissue [9]. Comparing the two creates an image of

blood perfusion in burn tissue. Hyperspectral imaging (HSI) also aims to look at blood perfusion, using wavelengths of light corresponding to unbound hemoglobin (Hb) and deoxyhemoglobin (HbO₂) to determine total amount of hemoglobin and the oxygen saturation of hemoglobin. Using NIR light as the illumination method, near infrared spectral imaging (NIRSI), researchers used light ranging from 950 to 1650 nm to create the image [11]. Training an AI model to look at these data, they found low error once the AI was looking at non-training data. Spatial frequency domain imaging (SFDI) looks at absorption parameters and light scattering parameters to understand structural features. Using these features, SFDI can look at Hb concentration, oxygen saturation, and collagen content. With machine learning, it was possible to predict burn severity with high accuracy. Machine learning has also been applied to camera photos to determine burn depth, and while less accurate at assessing depth, it had good success rates for assessing need for skin graft. Optical coherence tomography (OCT) uses NIR light to create 3D images similar to ultrasound. Using a polarization sensitive OCT, researchers were able to determine burn depth through collagen denaturation, while others have used OCT to look for structural changes in the skin. Finally, photoacoustic imaging (PAI) senses the expansion of chromophores in response to laser energy.

Table 1: Features of discussed methods to assess burn depth [9]

Method	Parameters of interest	Measured values	Results	Limitations
LDI	Wavelength change due to moving substances	Blood perfusion	Accuracy within 24 hrs 80.8%, on third day 92.3%	No universal standards on measurement parameters, long scanning time
LSI	Backscatter from laser change due to movement	Blood perfusion	Sensitivity and specificity 92.3% and 78.3% within 24 hrs, 100% and 90.4% on day 3	Measures change of movement in tissue, not just blood movement
HIS	Backscatter from LEDs at wavelengths corresponding to Hb and HbO ₂	Volume of all Hb, %HbO ₂ , blood perfusion	Sensitivity 92%, specificity 71% on day 3	Not many studies. Small sample sizes. Needs standards for children
NIRSI [11]	HSI image created from wavelengths ranging from 950 nm to 1650 nm	AI output	Average relative error 7%	
SFDI	Hb content, oxygen saturation, collagen content	AI output	Accuracy 92.5%	
Smart photos	Color, shape, texture, morphology	AI output	66.2% success for depth classification, 83.8% success for necessity of burn graft	Imaging devices, lighting conditions, and backgrounds could influence AI output
OCT	Polarization of light, images generated	Collagen denaturation, structural changes due to burn		Low imaging contrast for different tissue types
PAI	Blood vessel identification, Hb, albumin accumulation	Oedema	High correlation	Noise from skin surface can be hard to distinguish from blood signals

CHAPTER 2

BURN DEPTH AND SKIN HYDRATION

2.1 Jackson Thermal Wound Theory

In 1953, Jackson published his findings on the localized effects of contact and flame burns on surrounding tissue. Over 70 years later, his theory still stands and has been expanded to other burn causes, including friction and electrical burns. Below is a schematic of his theory.

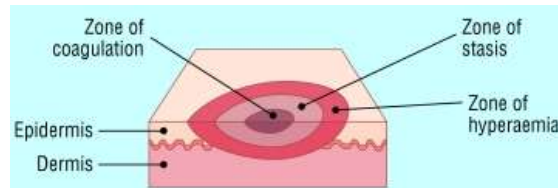


Figure 2: The zones of Jackson's thermal wound theory [2].

In the above image, the burn has damaged tissue in the zone of coagulation, causing protein denaturation and imminent necrosis of tissue. In a sphere around it, lies the zone of stasis, where the damage from the burn is less severe and there is no protein denaturation. Because of the cell death in the zone of coagulation and the proteins from that region leaking out to this region, it is harder for the body to send adequate fluids to this region. Should external resuscitation not be properly provided, this section of tissue will become part of the zone of coagulation itself. Outside of this is the zone of hyperaemia, where the body sends a significant amount of fluid to attempt to resuscitate the zones of stasis and coagulation. Largely undamaged by the burn injury itself, this region of tissue contains a lot of fluid and unless targeted by infection, will likely survive the burn injury without significant external help needed.

2.2 Other Examples of Water Loss from Burns

In extreme cases, where 30% or more of the body's surface area is covered in partial or full thickness burns, many systemic symptoms occur, known together as burn shock [2]. The below image describes some of these symptoms.

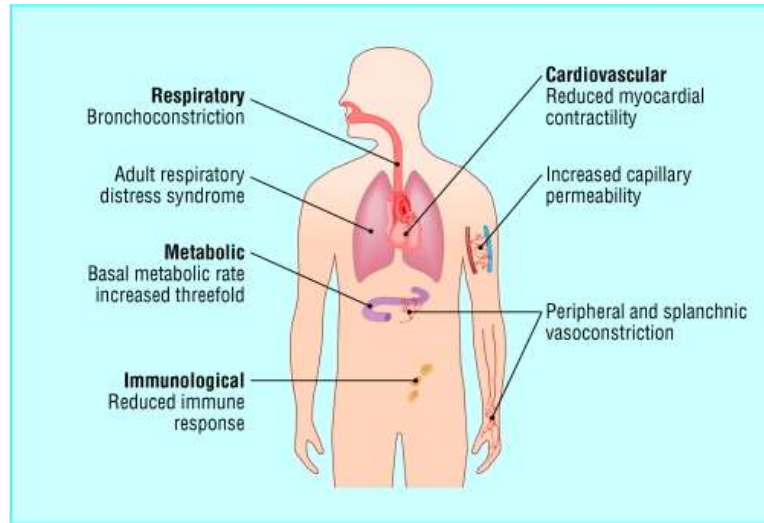


Figure 3: Some symptoms of burn shock [2].

Of particular interest is the increased leakiness in capillaries, suggesting that nutrients flow is increased in response to a significant part of the body being burned. Additionally, the vasoconstriction of the peripheral and abdominal regions suggests that blood volume is low, requiring remaining blood to be redistributed to vital systems (brain, lungs, and heart). This is also evident in the reduced contractility of the heart, as an increase in filling pressure is associated with an increase in contractility, therefore a lack of contractility would suggest a decrease in filling pressure. This shows that on a macroscopic level, burns lead to significant fluid loss, suggesting that in the local area, fluid loss might be an indicator of the severity of a burn injury.

2.3 Noninvasive Methods of Measuring Water Content

In order to decrease the amount of pain felt by a patient, it was determined that noninvasive measurement would be the optimal means of measuring skin water content. Early on this investigation, a review article was found, discussing many different optical and electrical methods of measuring skin hydration, as well as other previous methods discussed.

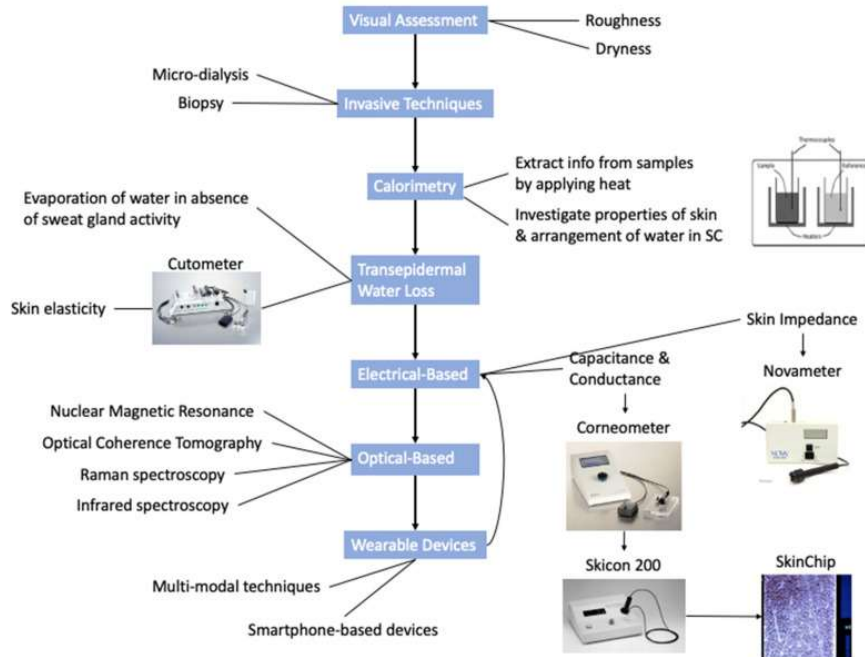


Figure 4: Methods of measuring skin hydration [3]. SC stands for stratum corneum, the uppermost layer of the epidermis

Many of the techniques discussed above may be inappropriate for burn patients, as a visual assessment looking for skin roughness and dryness might overlook those factors when looking at the burned skin of a patient. Using techniques that require contact with a patient's skin may cause further pain to the patient, so those methods were ruled out, leaving just optical-based devices. To reduce cost, it was decided that using a pair of LEDs at different wavelengths could feasibly function as a limited NIRS looking at just water absorption in the skin. The absorbance spectra of water and common chromophores are shown below, with wavelengths of interest marked.

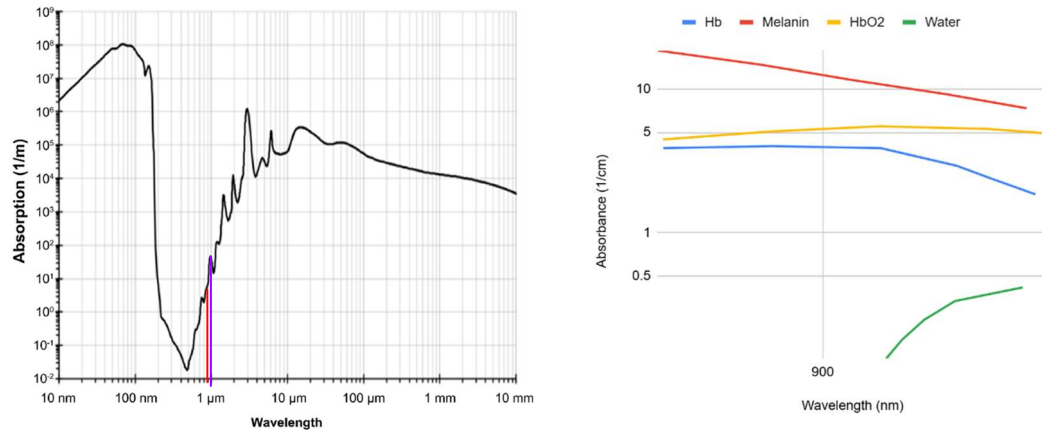


Figure 5: From left to right, absorption coefficients of liquid water [4] and the absorbance of chromophores in skin in the proposed range, adapted from [5]. In the rightmost image, the absorbance corresponds to the amount in tissue. Lines in red and purple indicate proposed wavelengths, with red at 910 and purple at 970 nm.

As shown above, 970 nm is an absorption peak in water, whereas 910 nm is a relatively stable value right before the peak. While melanin, Hb, and HbO₂ are decreasing between 910 and 970 nm by at most 5 cm⁻¹, water increases in absorbance by .4 cm⁻¹. there is no large difference in absorbance across the other chromophore values at these wavelengths, meaning that a change in the differential amount of light absorbed should mostly be due to changes in water content.

CHAPTER 3

PROPOSED DEVICE

3.1 Materials

To make the device function as planned, 2 LEDs are needed, one at 970 nm and the other at 910 nm. In order to collect signals from the LEDs, a silicon photodiode is needed to sense light reflecting back from the skin. These photodiodes were used because they are most responsive in the NIR region, as shown in the figure below.

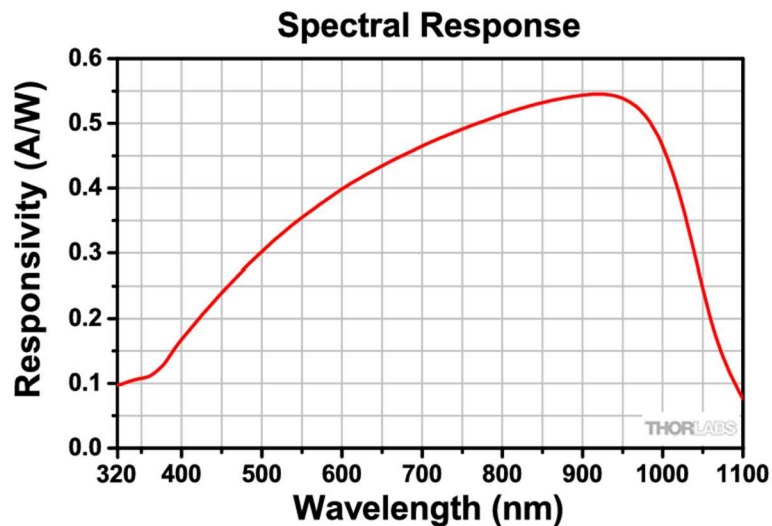


Figure 6: Responsivity graph of photodiodes used, provided in product information. [13]

To collect and interpret these signals, a microcontroller is used. Ideally, it would also run calculations based on the difference between the light collected when either LED is running to give an output in skin hydration on either an LCD screen or to send to a computer.

3.2 Circuit

Two different circuits were used in testing the device. The first used a voltage divider to step down the 5 volts from the microcontroller to a 1 volt bias voltage for the photodiode as shown below.

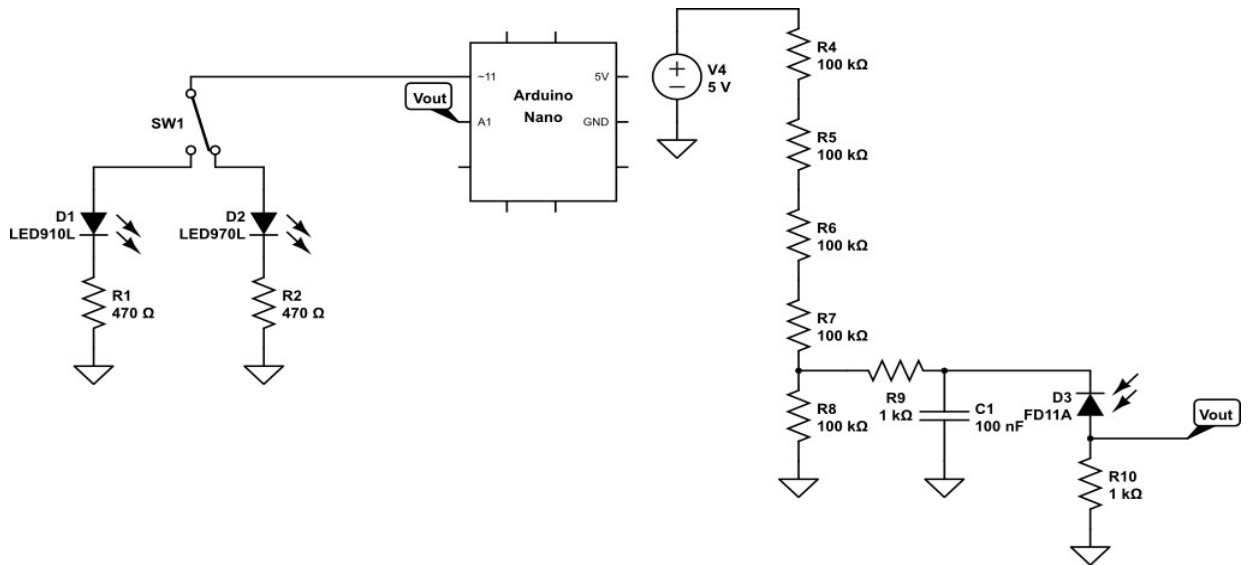


Figure 7: Original device circuit

Unfortunately, when validating the ability of the photodiode to recognize light from the LEDs, it was found that output voltage was negligible. As the rest of the photodiode circuit was recommended by the manufacturer, I had concluded that something went awry in the voltage divider. Using a voltage source as a 1-volt battery, I then modified the right half of the circuit, as shown below.

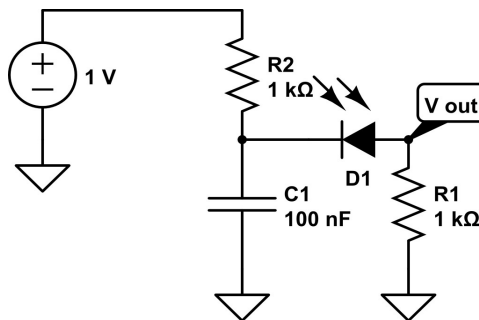


Figure 8: Modified photodiode circuit

With these changes, the voltage output was larger, but did not change much with the application of ambient light or light from either photodiode. With further testing, it might have been possible to determine the cause of this problem, however as this problem was found near the deadline, the root cause was not determined. Code used for testing can be found in appendix A.

CHAPTER 4

SAFETY OF PROPOSED METHOD

4.1 Introduction

To determine the safety of the proposed device, we ensured that all LEDs used followed standards, as discussed in [12]. There were three different standards from IEC-62471 looking at skin safety, cornea safety, and retina safety, ensuring safe operation.

4.2 Irradiance Equations

The equations for skin safety (1) and cornea safety (2, 3) were extremely similar, with the later having a stricter exposure limit, as seen below:

$$E_H = \sum_{\lambda=380}^{3000} \sum_t E_{\lambda}(\lambda, t) \Delta t \Delta \lambda \leq 20000 \cdot t^{-0.75} \text{W} \cdot \text{m}^{-2} (t \leq 10s) \quad (1)$$

$$E_H = \sum_{\lambda=780}^{3000} \sum_t E_{\lambda}(\lambda, t) \Delta t \Delta \lambda \leq 18000 \cdot t^{-0.75} \text{W} \cdot \text{m}^{-2} (t \leq 1000s) \quad (2)$$

$$E_{IR} = \sum_{\lambda=780}^{3000} E_{\lambda} \Delta \lambda \leq 100 \text{W} \cdot \text{m}^{-2} (t > 1000s) \quad (3)$$

In these equations, E_H is the exposure limit, E_{λ} is the spectral irradiance in $\text{W} \cdot \text{m}^{-2} \cdot \text{nm}^{-1}$, $\Delta \lambda$ is the bandwidth in nm, and t is exposure time in seconds.

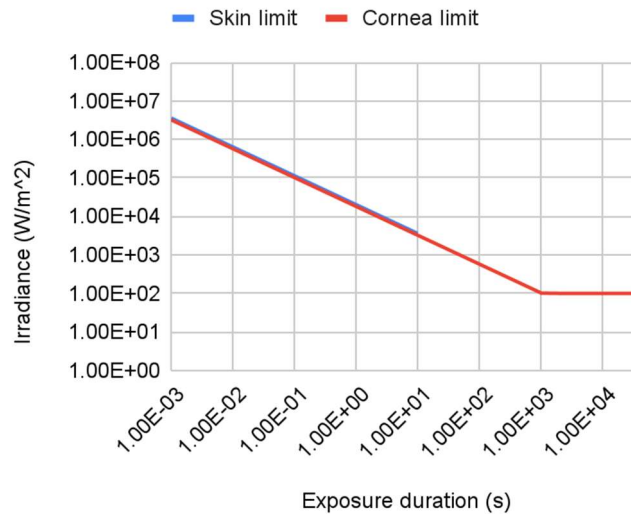


Figure 9: (1), (2), and (3) plotted

While these were simplified individually, in the interest of brevity, this will detail the simplification of (2). One of the first things done was convert the double summation to a double integral, creating the following lefthand section of the equation:

$$E_H = \int_{\lambda=780}^{3000} \int_t E_{\lambda}(\lambda, t) dt d\lambda \quad (4)$$

The LEDs were used in a non-pulsed manner and had a small bandwidth, allowing for the assumption to be made that E_{λ} is constant in t and limited in λ . These bring us to (5):

$$E_H = \int_{\lambda=780}^{3000} E_{\lambda}(\lambda, t) d\lambda \quad (5)$$

The product information for either LED did not provide an irradiance, however it did give optical power at various voltages in Watts, not Watts per nanometer, indicating that the spec sheet gave integrated power over all wavelengths (6)

$$P_{specs} = \int_{\lambda_{min}}^{\lambda_{max}} P(\lambda) d\lambda \quad (6)$$

Irradiance is defined as the optical power per unit area ($E = \frac{P}{A}$), plugging that in (5) brings (7)

$$E_H = \frac{I}{A} \int_{\lambda=780}^{3000} P(\lambda) d\lambda \quad (7)$$

With a wavelength spectrum within the range of the integral ($780 \leq \lambda_{min}, \lambda_{max} \leq 3000$), outside the spectrum the integral returns 0. This leaves the equation below:

$$E_H = \frac{I}{A} \int_{\lambda_{min}}^{\lambda_{max}} P(\lambda) d\lambda \quad (8)$$

Substituting (6) in (8) brings us to the simplification,

$$E_H = \frac{P_{specs}}{A} \quad (9)$$

for wavelengths within the integral, small bandwidth, and LEDs used in a non-pulsed manner.

4.2.1 Defining the Area

Using this for a biological purpose makes definition of the area difficult, this was simplified to assume that tissue was similar to a plane perpendicular to the mean light direction. Optical equations were used to determine the size of a circle illuminated by a point source a distance d away. Since the LEDs used had a glass ball lens, we used the equation:

$$EFL = \frac{nD}{4(n-1)} \quad (10)$$

where EFL is the effective focal length, D is the diameter of the ball lens, and n is the refractive index, estimated to be 1.5.

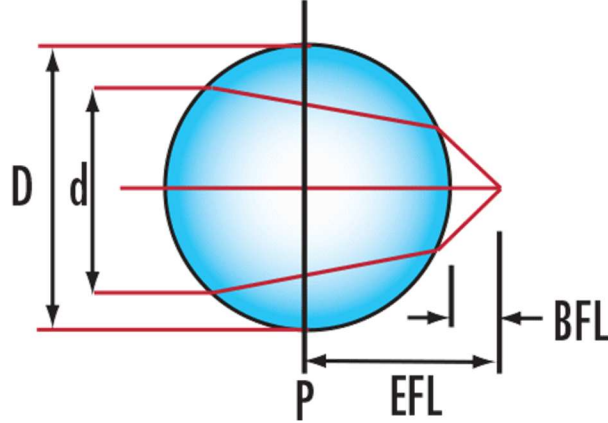


Figure 10: Pictorial representation of important variables used in (10) [6].

Once the focal distance was found, the CAD drawing on the product information was used to find the distance between the chip and the center of the ball lens, referred to as s , and plugged the focal distance f into the below equation to solve for i , or the distance between the lens and the virtual image.

$$\frac{1}{f} = \frac{1}{s} + \frac{1}{i} \quad (11)$$

Using the distance between the virtual image of the point source in the LED and the half angle, ϕ , where beyond which light from the source was practically negligible, we determined the radius of a circle lit by the lens at a distance d_v from the virtual image to be

$$r = d_v \tan \phi \quad (12)$$

Plugging (10) into the area of a circle equation, and then into (9) yielded

$$E_H = \frac{P_{specs}}{\pi d_v^2 \tan^2 \phi} \quad (13)$$

At this point, (13) was plugged into (1) and (2) to solve for the maximum safe exposure time, yielding

$$t_{skin} \leq \left(\frac{P}{\pi d_v^2 \tan^2 \phi \cdot 20000} \right)^{-1.33} \quad (14)$$

$$t_{cornea} \leq \left(\frac{P}{\pi d_v^2 \tan^2 \phi \cdot 18000} \right)^{-1.33} \quad (15)$$

Meanwhile, (3) was converted to

$$E_H = \frac{P_{specs}}{\pi d_v^2 \tan^2 \phi} \leq 100 \text{ W} \cdot \text{m}^{-2}, t < 1000\text{s} \quad (16)$$

To correct for distance, d_v was converted to a distance d from the LED tip to the surface, where i was the distance from the virtual image to the center of the lens calculated in (10), and r_{lens} was the radius of the ball lens. This yielded:

$$d = d_v - i - r_{lens} \quad (17)$$

These equations were coded into a spreadsheet, with various distances tested to ensure that exposure is safe in these conditions.

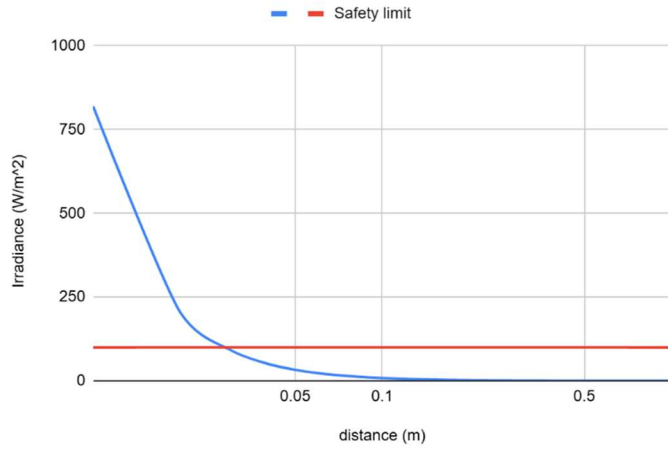


Figure 10: Irradiance per distance for an LED with a power of 16 mW and a dispersion angle of 14° , where distance is defined as that between the virtual image and the surface

4.3 Radiance Equations

The remaining pair of equations (18, 19) give the radiance limits for retina safety,

$$L_R = \sum_{\lambda=380}^{1400} L_\lambda \cdot R(\lambda) \cdot \Delta\lambda \leq \frac{50000}{\alpha \cdot t^{0.25}} \text{ W} \cdot \text{m}^{-2} \cdot \text{sr}^{-1} \quad (18)$$

$$L_{IR} = \sum_{\lambda=780}^{1400} L_\lambda \cdot R(\lambda) \cdot \Delta\lambda \leq \frac{6000}{\alpha} \text{ W} \cdot \text{m}^{-2} \cdot \text{sr}^{-1} (t > 10\text{s}) \quad (19)$$

where L_R and L_{IR} are the exposure limits for light exposure and infrared light exposure respectively, L_λ is the spectral radiance in $\text{W} \cdot \text{m}^{-2} \cdot \text{nm}^{-1} \cdot \text{sr}^{-1}$, $R(\lambda)$ is the burn weighting

function, $\Delta\lambda$ is the bandwidth in nm, t is exposure time in seconds, and α is defined as angular subtense in sr. Below α and $R(\lambda)$ are defined:

$$\alpha = \frac{(l+b)/2}{d} \leq 0.1 \text{ sr} \quad (20)$$

$$R(\lambda) = 10^{\frac{700-\lambda}{500}} \quad (21)$$

in which l and b are the length and breadth of the light source and d is the distance between the light source and item in question. α is restricted to less than 0.1 steradian due to the geometry of the eye. Radiance is likely used as a safety limit in a per retina cell capacity, as each cell has a limited angular range of information.

Since LEDs used were narrow bandwidth, the summation of all frequencies made little sense, bringing (18) to

$$L_R = L \cdot 10^{\frac{700-\lambda}{500}} \cdot \Delta\lambda \quad (22)$$

for $380 < \lambda < 1400$. The intensity was calculated at the LED, yielding the equation

$$I = \frac{P}{A_{LED}} \quad (23)$$

The irradiance was derived from the equation

$$L = I \times \Omega, \quad (24)$$

where Ω was the solid angle of the light source. To derive Ω , the angular intensity of the LEDs used, the following equation was used:

$$L = \frac{P}{A \times \Omega} = \int_{\theta=0}^{\pi} \int_{\phi}^{2\pi} L_0 \sin \theta \, d\phi d\theta \quad (25)$$

Solving for the inside integral, and using the angular intensity to limit the range of θ , with its maximum at ϕ_m led to the equation:

$$L = \frac{P}{A \times \Omega} = 2\pi L_0 \int_{\theta=0}^{\phi_m} \sin \theta \, d\theta, \quad (26)$$

which solved to

$$\frac{P}{A \times \Omega} = 2\pi L_0 (1 - \cos \phi_m) \quad (27)$$

Solving for the solid angle led to the equation:

$$L \cdot \Omega = \frac{P}{A} = \frac{P \cdot L \cdot \Omega}{A \cdot 2\pi L_0 (1 - \cos \phi_m)} \quad (28)$$

The burn function, R_λ was wavelength specific, and did not require any special derivation.

α , or the angular subtense, was given by the reference material as $\alpha = \frac{l+w}{2d}$ with α_{eff} having a different set of equations.

$$\alpha_{eff}(t) = \begin{cases} 0.0017, & t \leq 0.25 \\ 0.011 \sqrt{\frac{t}{10}}, & 0.25 \leq t \leq 10 \\ 0.011, & t \geq 10 \end{cases} \quad (29)$$

Plugging all of that in yielded the equation

$$L_R = \frac{P}{A_{LED}} \times 10^{\frac{700-\lambda}{500}} \cdot \Delta\lambda \cdot 2\pi(1 - \cos \phi_m) \leq \frac{50000}{\alpha \cdot t^{0.25}} \quad (30)$$

Solving for time led to

$$\left(\frac{\frac{P}{A_{LED}} \times 10^{\frac{700-\lambda}{500}} \cdot \alpha \cdot \Delta\lambda \cdot 2\pi(1 - \cos \phi_m)}{50000} \right)^{-4} \leq t. \quad (31)$$

Plugging in the specs from the manufacturer for each LED confirmed that both LEDs were safe per IEC-62471.

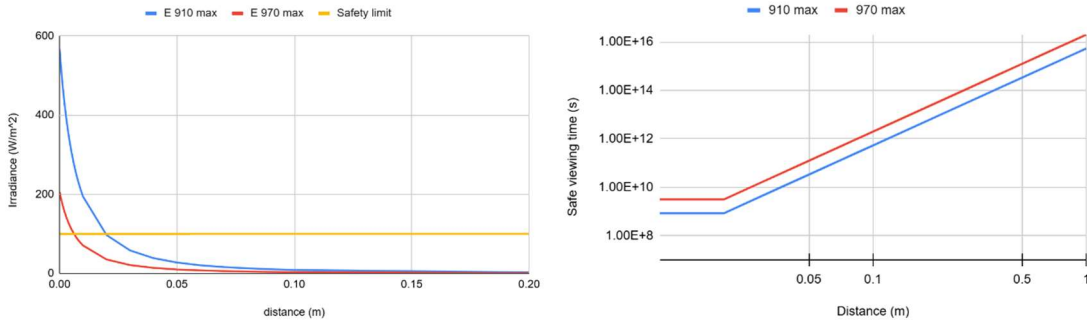


Figure 12: From left to right, the irradiance from the maximum optical power from each LED at various distances from tissue, the maximum amount of time considered to be safe to look at the LED per the radiance equations using values provided by the LED manufacturer at various distances from the eye.

CHAPTER 5

PLANNED TESTING

5.1 Hydration testing

Following the verification of the silicon photodetector, I planned to test whether this was a feasible method of sensing water. I had planned to start with comparing the readings from an empty container and the same container full of water. Should there have been little difference in readings, I planned to probe with a voltmeter to look for differences on the electrical side. If so, I would have implemented an operational amplifier (opamp) to increase the perceived voltage for the microcontroller.

Had this been successful, I would have followed it up with testing whether the device could still sense water when a substance covered it that had similar optical characteristics to skin. I would have incrementally increased the amount of the substance until it was no longer possible to differentiate between covered water and no water to determine the maximum detection range.

I would follow this up with testing the device on gelatin hydrogels with varying amounts of water in the formulation to attempt to find the type of relationship between differential light received and water concentration. At this point, I would ideally code a method that could approximate water hydration based on this measurement.

5.2 Skin testing

Assuming all prior testing went smoothly, I would then proceed to using a blowtorch to burn a skin-like substance and compare readings to that from the same substance when not burned. If there is a difference measured, burn depths would be simulated using layers of burned and unburned skin phantoms. For the device to be successful, it would need to be able to accurately find a difference between the partial and full thickness models.

5.3 Conclusion

The device uses light at two wavelengths associated with a water absorption peak. Subtracting the value of one from the other should reduce the background noise, while increasing the specificity of the signal. Using the silicon photodiode to measure these values should have been able to translate the optical power of the light to a current that could be sensed by a microcontroller. With fine tuning, this part should be able to sense the presence of water. While penetration depth is still unknown, as the LEDs and ambient light sources failed to produce a sizable change in the current produced by the photodiode, if it were able to penetrate into the dermis (about 1 cm thick), the device could be useful in diagnostics and patient checkups, especially in cases of patients needing fluid resuscitation due to shock or sepsis. While there are formulas for the amount of fluid needed for a patient with burn shock and other severe loss of fluids, being able to measure the fluids entering the patient in real time could reduce the number of patients who either do not receive enough fluids, or receive way too much and are unable to get rid of the excess. Tools like this could work in conjunction with such established methods of determining fluids necessary for a patient to help deal with individual differences.

Assuming that the device was not only able to penetrate into the dermis, but also see into the subcutaneous tissue, it is more than possible that such a device may be able to see changes in water content related to a burn, helping medical practitioners be able to assess burn depth and determine whether a graft is necessary for healing. Additionally, such a device can be produced cheaply and does not require internet connection to function, meaning that use in remote places would be possible, even without Wi-Fi or data.

BIBLIOGRAPHY

- [1] “What Do I Do About Burns?,” Cleveland Clinic. Accessed: May 12, 2025. [Online]. Available: <https://my.clevelandclinic.org/health/diseases/12063-burns>
- [2] S. Hettiaratchy and P. Dziejewski, “Pathophysiology and types of burns,” *BMJ*, vol. 328, no. 7453, pp. 1427–1429, Jun. 2004, doi: 10.1136/bmj.328.7453.1427.
- [3] I. M. Gidado, M. Qassem, I. F. Triantis, and P. A. Kyriacou, “Review of Advances in the Measurement of Skin Hydration Based on Sensing of Optical and Electrical Tissue Properties,” *Sensors*, vol. 22, no. 19, p. 7151, Sep. 2022, doi: 10.3390/s22197151.
- [4] “Coherence Field Theory: Quantum Coherence as the Basis for a Model of Brain Function,” ResearchGate. Accessed: May 12, 2025. [Online]. Available: https://www.researchgate.net/publication/363095974_Coherence_Field_Theory_Quantum_Coherence_as_the_Basis_for_a_Model_of_Brain_Function
- [5] D. Li, Y.-L. He, and G.-X. Wang, “Thermal Modelling for Laser Treatment of Port Wine Stains,” 2011. doi: 10.5772/19830.
- [6] “Understanding Ball Lenses.” Accessed: May 12, 2025. [Online]. Available: <https://www.edmundoptics.com/knowledge-center/application-notes/optics/understanding-ball-lenses/>
- [7] C. Cairns and K. Kang, “National Hospital Ambulatory Medical Care Survey: 2021 Emergency Department Summary Tables”, [Online]. Available: https://www.cdc.gov/nchs/data/nhamcs/web_tables/2021-nhamcs-ed-web-tables-508.pdf
- [8] T. R. Resch, R. M. Drake, S. D. Helmer, G. D. Jost, and J. S. Osland, “Estimation of Burn Depth at Burn Centers in the United States: A Survey,” *J. Burn Care Res.*, vol. 35, no. 6, pp. 491–497, Nov. 2014, doi: 10.1097/BCR.000000000000031.
- [9] H. Li, Q. Bu, X. Shi, X. Xu, and J. Li, “Non-invasive medical imaging technology for the diagnosis of burn depth,” *Int. Wound J.*, vol. 21, no. 1, p. e14681, 2024, doi: 10.1111/iwj.14681.
- [10] H. Hoeksema *et al.*, “A new, fast LDI for assessment of burns: A multi-centre clinical evaluation,” *Burns*, vol. 40, no. 7, pp. 1274–1282, Nov. 2014, doi: 10.1016/j.burns.2014.04.024.
- [11] P. Wang *et al.*, “Full-field burn depth detection based on near-infrared hyperspectral imaging and ensemble regression,” *Rev. Sci. Instrum.*, vol. 90, no. 6, p. 064103, Jun. 2019, doi: 10.1063/1.5034503.
- [12] “AB191-4 LUXEON IR Family Eye Safety Application Brief.” Accessed: Apr. 19, 2025. [Online]. Available: <https://otmm.lumileds.com/adaptivemedia/17897dc0449b31dfd49e3f49b465795f6d58285e>
- [13] “Thorlabs - FD11A Si Photodiode, 400 ns Rise Time, 320 - 1100 nm, 1.1 mm x 1.1 mm Active Area.” Accessed: May 15, 2025. [Online]. Available: <https://www.thorlabs.com>

APPENDIX A

CODE USED IN EXPERIMENTS

```
const int led=11; //on PWM
#define sense A1
float Vin=5;
//float Vin=3.3;
int in=5;
const int l=0;
const int t=10000; //delay time of 10s
int n=1;

//Will be using PWM
void setup() {
  Serial.begin(9600);
  pinMode(led, OUTPUT);
  digitalWrite(led,LOW);
}

void loop() {
  Serial.print(n);
  analogWrite(led,n);
  int I=analogRead(sense);
  Serial.println(I);
  n=n+in;
  if(n>255)
  {
    n=n-255;
  }
  delay(t);
}
```

APPENDIX B

LIST OF EQUATIONS

B.1 Equations from IEC-62471

$$E_H = \sum_{\lambda=380}^{3000} \sum_t E_{\lambda}(\lambda, t) \Delta t \Delta \lambda \leq 20000 \cdot t^{-0.75} \text{W} \cdot \text{m}^{-2} (t \leq 10\text{s}) \quad (1)$$

$$E_H = \sum_{\lambda=780}^{3000} \sum_t E_{\lambda}(\lambda, t) \Delta t \Delta \lambda \leq 18000 \cdot t^{-0.75} \text{W} \cdot \text{m}^{-2} (t \leq 1000\text{s}) \quad (2)$$

$$E_{IR} = \sum_{\lambda=780}^{3000} E_{\lambda} \Delta \lambda \leq 100 \text{W} \cdot \text{m}^{-2} (t > 1000\text{s}) \quad (3)$$

$$L_R = \sum_{\lambda=380}^{1400} L_{\lambda} \cdot R(\lambda) \cdot \Delta \lambda \leq \frac{50000}{\alpha \cdot t^{0.25}} \text{W} \cdot \text{m}^{-2} \cdot \text{sr}^{-1} \quad (18)$$

$$L_{IR} = \sum_{\lambda=780}^{1400} L_{\lambda} \cdot R(\lambda) \cdot \Delta \lambda \leq \frac{6000}{\alpha} \text{W} \cdot \text{m}^{-2} \cdot \text{sr}^{-1} (t > 10\text{s}) \quad (19)$$

$$\alpha = \frac{(l+b)/2}{d} \leq 0.1 \text{ sr} \quad (20)$$

$$R(\lambda) = 10^{\frac{700-\lambda}{500}} \quad (21)$$

$$\alpha_{eff}(t) = \begin{cases} 0.0017, & t \leq 0.25 \\ 0.011 \sqrt{\frac{t}{10}}, & 0.25 \leq t \leq 10 \\ 0.011, & t \geq 10 \end{cases} \quad (29)$$

B.2 Optical equations

$$EFL = \frac{nD}{4(n-1)} \quad (10)$$

$$\frac{1}{f} = \frac{1}{s} + \frac{1}{i} \quad (11)$$

$$L = I \times \Omega \quad (24)$$